The Astrophysical Journal, 649:640–648, 2006 October 1
© 2006. The American Astronomical Society. All rights reserved. Printed in U.S.A.

EVOLUTION OF X-RAY CLUSTER SCALING RELATIONS IN SIMULATIONS WITH RADIATIVE COOLING AND NONGRAVITATIONAL HEATING

Orrarujee Muanwong,[1] Scott T. Kay,[2,3] and Peter A. Thomas[3]

Received 2005 September 26; accepted 2006 May 25

ABSTRACT

We investigate the redshift dependence of X-ray cluster scaling relations drawn from three hydrodynamic simulations of the ΛCDM cosmology: a "Radiative" model that incorporates radiative cooling of the gas, a "Preheating" model that additionally heats the gas uniformly at high redshift, and a "Feedback" model that self-consistently heats cold gas in proportion to its local star formation rate. While all three models are capable of reproducing the observed local L_X-T_X relation, they predict substantially different results at high redshift (to $z = 1.5$), with the Radiative, Preheating, and Feedback models predicting strongly positive, mildly positive, and mildly negative evolution, respectively. The physical explanation for these differences lies in the structure of the intracluster medium. All three models predict significant temperature fluctuations at any given radius due to the presence of cool subclumps and, in the case of the Feedback simulation, reheated gas. The mean gas temperature lies above the dynamical temperature of the halo for all models at $z = 0$, but differs between models at higher redshift, with the Radiative model having the lowest mean gas temperature at $z = 1.5$. We have not attempted to model the scaling relations in a manner that mimics the observational selection effects, nor has a consistent observational picture yet emerged. Nevertheless, evolution of the scaling relations promises to be a powerful probe of the physics of entropy generation in clusters. First indications are that early, widespread heating is favored over an extended period of heating, as is associated with galaxy formation.

Subject headings: cosmology: theory — galaxies: clusters: general — X-rays: galaxies: clusters

Online material: color figures

1. INTRODUCTION

X-ray scaling relations of galaxy clusters, namely the temperature-mass, T_X-M relation and the luminosity-temperature, L_X-T_X relation, play a pivotal role when using the abundance of clusters to constrain cosmological parameters (Henry & Arnaud 1991; White et al. 1993; Eke et al. 1996; Viana & Liddle 1996, 1999; Henry 1997, 2000, 2004; Borgani et al. 2001; Pierpaoli et al. 2001, 2003; Seljak 2002; Viana et al. 2003; Allen et al. 2003). It is well known, however, that accurate calibration of scaling relations is crucial for avoiding a major source of systematic error. For example, the T_X-M relation is widely used by many of these authors to constrain the amplitude of mass fluctuations, conventionally defined using the parameter σ_8. Systematic deviations in the normalization of the T_X-M relation, particularly due to how cluster mass is estimated (e.g., see Horner et al. 1999), are amplified by the steep slope of the temperature function, leading to large variations in σ_8 (see Henry 2004 for a discussion of recent results).

As far as the L_X-T_X relation is concerned, the discrepancies are more prominent, as L_X is highly sensitive to the thermodynamics of the of the inner intracluster medium (ICM) and can yield different values for both normalizations and slopes (Edge & Stewart 1991; White et al. 1997; Allen & Fabian 1998; Markevitch 1998; Xue & Wu 2000). The situation is further complicated by the fact that clusters do not scale self-similarly, as would be the case (approximately) if the only source of heating were via gravitational infall (Kaiser 1986). This makes the problem more difficult to investigate theoretically, although it allows studies of cluster scaling relations to reveal more information on the physics governing the structure of the intracluster medium.

The departure from self-similarity can be attributed to an increase in the entropy of the gas, which particularly affects low-mass systems (Evrard & Henry 1991; Kaiser 1991; Bower 1997; Tozzi & Norman 2001; Ponman et al. 1999; Voit & Bryan 2001; Voit et al. 2002, 2003). Many theoretical studies have been performed to investigate the effects of various physical processes that can raise the entropy of the gas, based on models involving heating (Metzler & Evrard 1994; Balogh et al. 1999; Kravtsov & Yepes 2000; Loewenstein 2000; Wu et al. 2000; Bower et al. 2001; Borgani et al. 2002), radiative cooling (Knight & Ponman 1997; Pearce et al. 2000; Bryan 2000; Muanwong et al. 2001, 2002, hereafter MTKP02; Davé et al. 2002; Wu & Xue 2002), and a combination of the two (MTKP02; Kay et al. 2003, 2004, hereafter KTJP04; Tornatore et al. 2003; Valdarnini 2003; Borgani et al. 2004; McCarthy et al. 2004).

Measurements of how cluster scaling relations evolve with redshift allow even tighter constraints to be placed on cosmological parameters (and entropy generation models), and observations of cluster properties at high redshift are now starting to become available, owing primarily to the high sensitivity of *Chandra* and *XMM-Newton*. From a theoretical point of view, this is an exciting phase, as we can now fully exploit the availability of our simulated distant clusters and compare their X-ray properties with real observations. It is therefore timely to investigate further the effects of entropy generation on the evolution of cluster scaling relations as the available data for high-redshift systems accumulates.

In this paper, we will use cosmological hydrodynamical simulations described in MTKP02, and in KTJP04, to trace the evolution of the cluster population to high redshift ($z = 1.5$). Our results will primarily focus on three ("Radiative," "Preheating," and "Feedback") models, all able to reproduce the local L_X-T_X relation. The aims of this paper are to determine how the scaling

[1] Department of Physics, Faculty of Science, Khon Kaen University, Khon Kaen, 40002, Thailand; orrmua@kku.ac.th.

[2] Astrophysics, Denys Wilkinson Building, Keble Road, University of Oxford, Oxford, OX1 3RH, UK.

[3] Astronomy Centre, Department of Physics and Astronomy, School of Science and Technology, University of Sussex, Falmer, Brighton, BN1 9QH, UK.

relations evolve with redshift in the three models and to discover what the evolution of scaling relations can teach us about nongravitational processes occurring in clusters.

The rest of this paper is outlined as follows. In § 2 we introduce the X-ray scaling relations and summarize our present observational knowledge of these quantities. Details of our simulated cluster populations are presented in § 3. In § 4 we present our main results, first at $z = 0$, where the models are in good agreement with each other and the observations, then as a function of redshift, where the models predict widely different results. We discuss the implications of these differences in § 5 and demonstrate that the degree of X-ray evolution is driven by the supply of cold, low entropy gas. Finally, we summarize our conclusions in § 6.

2. X-RAY CLUSTER SCALING RELATIONS

Kaiser (1986) derived the following relations for temperature

$$T_X \propto M^{2/3}(1+z), \tag{1}$$

and luminosity

$$L_X \propto M^{4/3}(1+z)^{7/2} \tag{2}$$

$$\propto T_X^2(1+z)^{3/2}, \tag{3}$$

assuming the distribution of gas and dark matter in clusters is perfectly self-similar and the X-ray emission is primarily thermal bremsstrahlung radiation. Observed clusters do not form a self-similar population, but it is nevertheless convenient to describe their behavior using a generalized power-law form:

$$Y = C_0(z)X^{\alpha} = Y_0 X^{\alpha}(1+z)^{A}, \tag{4}$$

where $C_0(z)$ and Y_0 determine the normalization, α is the slope of the relation (in log space) and A determines how the relation evolves with redshift. Our main results will focus on the determination of A.

Observationally, attempts to measure the T_X-M relation at high redshift are currently in their infancy, as they require temperature profiles to be measured so that their mass can be estimated, but initial results are consistent with self-similar evolution ($A \sim 1$; Maughan et al. 2005; Kotov & Vikhlinin 2005).

Measuring the L_X-T_X relation at higher redshift is a somewhat simpler prospect, and has been attempted by many authors (Mushotzky & Scharf 1997; Fairley et al. 2000; Holden et al. 2002; Novicki et al. 2002; Arnaud et al. 2002; Vikhlinin et al. 2002; Lumb et al. 2004; Ettori et al. 2004; Maughan et al. 2005; Kotov & Vikhlinin 2005). We summarize recent results that adopt a low-density flat cosmology in Figure 1, attempting to include in the size of the error bars the uncertainty in A due to the choice of local relation (when quoted by the authors). Although the present situation is by no means clear, taking all results at face value generally favors positive evolution ($0 \lesssim A \lesssim 2$) with the latest results being consistent with self-similar evolution ($A = 3/2$). Larger samples of high redshift clusters (such as that expected from the *XMM-Newton* Cluster Survey; Romer et al. 2001) will be crucial to accurately constrain the degree of evolution in the L_X-T_X relation.

3. SIMULATED CLUSTER POPULATIONS

Our results are drawn from three similarly sized N-body/smooth particle hydrodynamics (SPH) simulations of the ΛCDM cosmology, which have already been published in MTKP02 and KTJP04. The simulation box in MTKP02 has a comoving side of

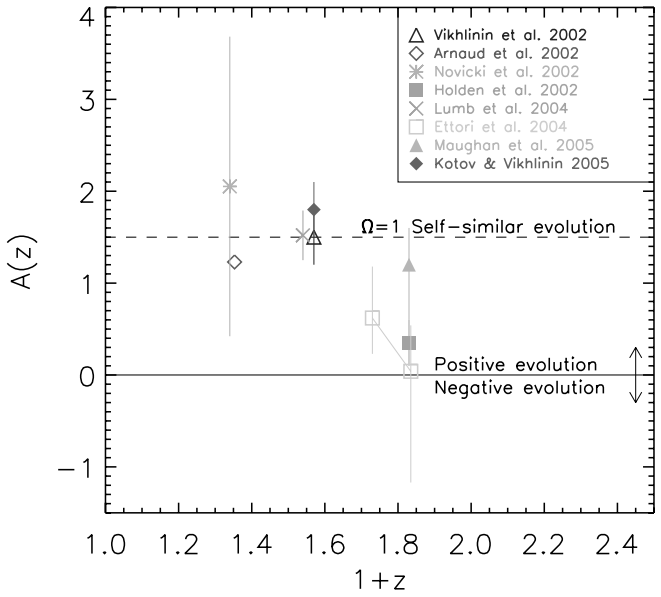

FIG. 1.—Evolution in the L_X-T_X relation as measured from various high-redshift cluster samples. [*See the electronic edition of the Journal for a color version of this figure*.]

100 h^{-1} Mpc with 160^3 particles each of gas and dark matter, whose particle masses are set to 2.6×10^9 and $2.1 \times 10^{10}\ h^{-1}\ M_\odot$, respectively. The box used in KTJP04 is bigger, with a side of 120 h^{-1} Mpc using 256^3 particles each of gas and dark matter, whose particle masses are 1.3×10^9 and $7.3 \times 10^9\ h^{-1}\ M_\odot$, respectively. Full details can be found in the articles. The key difference between the simulations is the model used to raise the entropy of the intracluster gas, summarized as follows:

1. A Radiative model where the excess entropy originated from the removal of low entropy gas to form stars, causing higher entropy gas to flow adiabatically into the core from larger radii (MTKP02).

2. A Preheating model where entropy was generated impulsively by uniformly heating the gas by 1.5 keV per particle at $z = 4$ (MTKP02).

3. A Feedback model where the entropy of (on average) 10% of cooled gas in high density regions was raised by 1000 keV cm^2, mimicking the effects of heating due to stars and active galactic nuclei (KTJP04).

These three models differ in the timing and distribution of entropy generation in the intracluster medium. The Radiative model has no explicit feedback of energy but relies on the removal of low-entropy gas via cooling; as such, it represents a minimal heating model. The Preheating model contains distributed heating at high redshift such as might occur if entropy generation occurs mainly in low-mass galaxies. By contrast heating in the Feedback model occurs solely in high-density regions. In all our models, there is very little star formation before a redshift of $z = 4$, after which the star formation rate (SFR) begins to rise rapidly. In the Preheating simulation, the SFR is then strongly suppressed, whereas in the other two simulations it peaks at a redshift of $z = 2$ and then declines back down to low values by the present day, with a time variation that matches that of the star formation history of the universe. The global baryon fraction in stars (and cold gas) at $z = 0$ is 0.002, 0.076, and 0.127 in the Preheating , Radiative and Feedback simulations, respectively. The largest of these corresponds to a stellar mass density of $\Omega_* = 0.006$; thus none of the models have excessive star formation.

These models are far from exhaustive, and their precise details should not be taken too seriously. The purpose of this paper is not to examine particular models but to illustrate that the evolution of the X-ray scaling relations can provide a powerful discriminant between different classes of model.

3.1. *Cluster Identification and Properties*

Clusters were selected at four redshifts ($z = 0, 0.5, 1$, and 1.5) using the procedure outlined in MTKP02. They are defined to be spheres of matter, centered on the dark matter density maximum, with total mass

$$M_\Delta = \frac{4}{3}\pi R_\Delta^3 \Delta \rho_{c0}(1+z)^3, \tag{5}$$

where $\rho_{c0} = 3H_0^2/8\pi G$ is the critical density at $z = 0$. We set $\Delta = 500$, as it corresponds to a sufficiently large radius such that the results are not dominated by the core, as well as corresponding approximately to the extent of current X-ray observations. Furthermore, as was shown by Rowley et al. (2004), the X-ray properties of simulated clusters within an overdensity of 500 exhibit less scatter than within the virial radius. Our choice of scaling with redshift[4] is independent of cosmology and would allow the simple power-law scalings to be recovered (eqs. [1], [2], and [3]) if the clusters were structurally self-similar.

We consider scaling relations involving mass, three measures of temperature, and luminosity for particle properties averaged within R_{500}. The mass

$$M_{500} = \sum_i m_i, \tag{6}$$

where the sum runs over all particles, of mass m_i. The dynamical temperature

$$kT_{\rm dyn} = \frac{\sum_{i,\,\rm gas} m_i kT_i + \alpha \sum_i (1/2) m_i v_i^2}{\sum_i m_i}, \tag{7}$$

where $\alpha = (2/3)\mu m_{\rm H} \sim 4.2 \times 10^{-16}$ keV for a fully ionized primordial plasma, assuming the ratio of specific heats for a monatomic ideal gas, $\gamma = 5/3$, and the mean atomic weight of a zero-metallicity gas, $\mu m_{\rm H} = 10^{-24}$ g. The first sum in the numerator runs over all gas particles, of temperature T_i, whereas the second sum runs over particles of all types with speed v_i, as measured in the center of momentum frame of the cluster.

We also consider the mass-weighted temperature of hot ($T > 10^5$ K) gas:

$$kT_{\rm gas} = \frac{\sum_{i,\,\rm hot} m_i kT_i}{\sum_{i,\,\rm hot} m_i}; \tag{8}$$

and we approximate the X-ray temperature of a cluster using the bolometric emission-weighted temperature:

$$kT_{\rm bol} = \frac{\sum_{i,\,\rm hot} m_i \rho_i \Lambda_{\rm bol}(T_i, Z) T_i}{\sum_{i,\,\rm hot} m_i \rho_i \Lambda_{\rm bol}(T_i, Z)}, \tag{9}$$

where ρ_i is the density and $\Lambda_{\rm bol}$ is the bolometric cooling function used in our simulations (Sutherland & Dopita 1993); for the Radiative and Preheating runs, $Z = 0.3(t/t_0)\ Z_\odot$ (MTKP02), and for the Feedback run, $Z = 0.3\ Z_\odot$ (KTJP04). Finally, the X-ray luminosity is approximated by the bolometric emission-weighted luminosity:

$$L_{\rm bol} = \sum_{i,\,\rm hot} \frac{m_i \rho_i \Lambda_{\rm bol}(T_i, Z)}{(\mu m_{\rm H})^2}. \tag{10}$$

It has been shown recently that the emission-weighted temperature is not an accurate diagnostic of cluster temperature, overpredicting the spectroscopic temperature by ~20%–30% when the emission is predominantly thermal bremsstrahlung (Mazzotta et al. 2004; Rasia et al. 2005). At lower temperatures ($kT < 3$ keV), line emission from heavy elements makes the problem significantly more complicated (Vikhlinin 2005). The volume sampled by our simulations ($\sim 100\,h^{-1}$ Mpc) means that we have very few clusters with $T > 3$ keV, and so a more accurate measure of the cluster temperature would require significantly more effort than applying a simple formula to our data. We therefore leave such improvements to future work, when larger samples of simulated clusters are available. It does not affect the conclusions of this paper.

TABLE 1
Numbers of Clusters at Various Redshifts

Relation	Redshift 0.0	0.5	1.0	1.5
Radiative Model				
Total	340	190	85	31
$T_{\rm dyn}$-M_{500}	330	186	84	31
$T_{\rm gas}$-M_{500}	332	186	82	31
$T_{\rm bol}$-M_{500}	319	151	64	24
$L_{\rm bol}$-M_{500}	317	186	85	31
$L_{\rm bol}$-$T_{\rm bol}$	256	95	34	14
Preheating Model				
Total	283	147	59	22
$T_{\rm dyn}$-M_{500}	273	143	56	22
$T_{\rm gas}$-M_{500}	271	143	56	22
$T_{\rm bol}$-M_{500}	264	134	53	22
$L_{\rm bol}$-M_{500}	269	143	59	22
$L_{\rm bol}$-$T_{\rm bol}$	190	92	48	14
Feedback Model				
Total	342	98	45	13
$T_{\rm dyn}$-M_{500}	328	96	43	12
$T_{\rm gas}$-M_{500}	327	89	41	11
$T_{\rm bol}$-M_{500}	305	90	39	10
$L_{\rm bol}$-M_{500}	339	98	45	13
$L_{\rm bol}$-$T_{\rm bol}$	269	67	32	12

3.2. *Cluster Catalogs*

Table 1 lists the numbers of clusters in our catalogs for each of the simulations at all four redshifts. The first row for each model gives the total number of clusters in our catalogs, down to a minimum mass, $M_{500} = 1.2 \times 10^{13}\ h^{-1}\ M_\odot$, corresponding to ~500 dark matter particles in the Radiative and Preheating simulations, and ~1400 dark matter particles in the (higher resolution) Feedback simulation. At $z = 0$, each model contains around 300 clusters above our mass limit, decreasing by around an order of magnitude by $z = 1.5$.

[4] Many authors prefer to adopt the redshift scaling of the critical density, $E(z)^2 = \Omega_m(1+z)^3 + \Omega_\Lambda$ (for a flat universe), rather than the background density, $(1+z)^3$.

We also made a number of additional cuts to the catalogs, specific to each scaling relation. Firstly, we noted a small number of systems that were significantly offset from the mean relation. On inspection, such objects were found to be erroneous, as they were subclumps falling into neighboring clusters. Thus, for each relation, we discarded all objects with $\Delta \log(Y) > 0.1$ (larger than intrinsic scatter in the $T_{\rm dyn}$-M_{500}, $T_{\rm gas}$-M_{500}, and $T_{\rm bol}$-M_{500} relations) and $\Delta \log(Y) > 0.5$ in the $L_{\rm bol}$-M_{500} and $L_{\rm bol}$-$T_{\rm bol}$ relations, respectively. Secondly, for the $L_{\rm bol}$-$T_{\rm bol}$ relation, we made an additional cut in temperature, such that the catalogs were complete in $T_{\rm bol}$ (excluding those clusters classed as outliers). For the Radiative model, the minimum temperatures are $kT_{\rm bol,\,min} = [0.74, 1.0, 1.25, 1.35]$ keV; for the Preheating model, $kT_{\rm bol,\,min} = [0.70, 0.96, 1.1, 1.37]$ keV; and for the Feedback model, $kT_{\rm bol,\,min} = [0.59, 1.12, 1.31, 1.58]$ keV, for $z = [0, 0.5, 1, 1.5]$. The numbers of clusters remaining in each of the relations after these cuts are also listed in Table 1.

4. RESULTS

4.1. *Scaling Relations at Redshift Zero*

We first present the scaling relations at $z = 0$, as they will form the basis for measuring evolution in the cluster properties with redshift. The parameters α and $C_0(0)$ listed in Table 2 are determined from the best least-squares fit to the relation

$$\log Y = \log C_0(0) + \alpha \log X, \qquad (11)$$

where X and Y represent the appropriate data sets in units of $10^{14}\ h^{-1}\ M_\odot$, 1 keV, and $10^{42}\ h^{-2}$ ergs s^{-1} for mass, temperature, and luminosity, respectively. We will consider each relation in turn.

Figure 2 illustrates the $T_{\rm dyn}$-M_{500} relation for each of the three simulations at $z = 0$, with best-fit relations overplotted as straight lines. The dynamical temperature is dominated by the contribution from the more massive dark matter particles, and so the resulting three relations are almost identical. The measured slope of the relation is $\alpha \sim 0.7$ (Table 2), which is close to, but slightly larger than, the self-similar value ($\alpha = 2/3$); this deviation is due to the variation of concentration with cluster mass. When the mass-weighted temperature of hot gas is used instead, the relation becomes flatter than the self-similar prediction, with $\alpha \sim 0.6$. This is expected, as the excess entropy generation due to cooling and heating is more effective in lower mass clusters (MTKP02).

TABLE 2
BEST-FIT SCALING RELATIONS

Relation	Model	α	$\log C_0(0)$	$\log Y_0$	A
$T_{\rm dyn}$-M_{500}	Radiative	0.70	0.34	0.34	1.1
	Preheating	0.70	0.33	0.33	1.1
	Feedback	0.69	0.33	0.33	1.2
$T_{\rm gas}$-M_{500}	Radiative	0.61	0.33	0.33	0.9
	Preheating	0.61	0.35	0.35	0.9
	Feedback	0.61	0.35	0.35	1.1
$T_{\rm bol}$-M_{500}	Radiative	0.59	0.38	0.37	0.5
	Preheating	0.61	0.35	0.35	0.8
	Feedback	0.64	0.33	0.33	1.2
$L_{\rm bol}$-M_{500}	Radiative	1.82	1.36	1.36	3.9
	Preheating	1.92	1.40	1.39	3.1
	Feedback	2.10	1.40	1.40	3.2
$L_{\rm bol}$-$T_{\rm bol}$	Radiative	3.06	0.19	0.20	1.9
	Preheating	3.05	0.26	0.24	0.7
	Feedback	3.13	0.28	0.28	−0.6

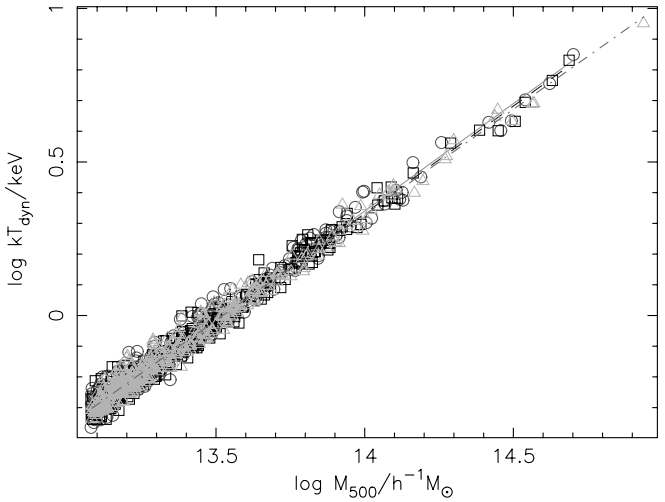

FIG. 2.—Dynamical temperature-mass relation within R_{500} at $z = 0$. Radiative clusters are plotted as circles (*with the solid line denoting the best-fit relation*), Preheating as squares (*dashed line*) and Feedback as triangles (*dash-dotted line*). [*See the electronic edition of the Journal for a color version of this figure.*]

Shown in Figure 3 is the $T_{\rm bol}$-M_{500} relation for each of the three models. Cool, dense gas dominates $T_{\rm bol}$ and so this temperature is more susceptible to fluctuations caused by merging substructure, leading to an increase in the scatter when compared to Figure 2. Again, the slope is flatter than the self-similar prediction, due to the effects of excess entropy. Differences between the models are larger than for the dynamical temperature but are less than the intrinsic scatter.

Finally, we consider relations involving the bolometric luminosity of the cluster. Fitting the relation between luminosity and mass, we find a slope in the range $\alpha \sim 1.8$–2.1, significantly steeper than the self-similar prediction ($\alpha = 4/3$). The departure from self-similarity is exacerbated when we plot bolometric luminosity against temperature (Fig. 4). Here, $\alpha \sim 3.1$ in all models, compared to $\alpha = 2$ for the self-similar case. The $L_{\rm bol}$-$T_{\rm bol}$ relations from the three simulations are in reasonable agreement with one another and in good agreement with the observed luminosity-temperature relation (see MTKP02; KTJP04).

In summary, all three models successfully generate excess entropy in order to break self-similarity at the level required by

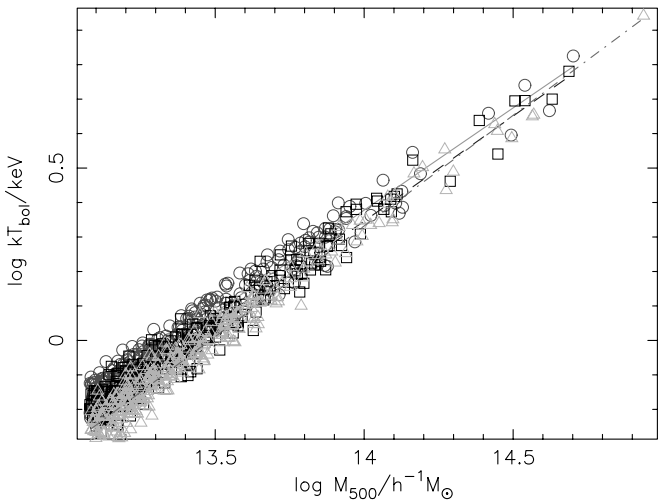

FIG. 3.—Bolometric emission-weighted temperature-mass relation within R_{500} at $z = 0$ for clusters in the three simulations. Symbols and lines are as in Fig. 2. [*See the electronic edition of the Journal for a color version of this figure.*]

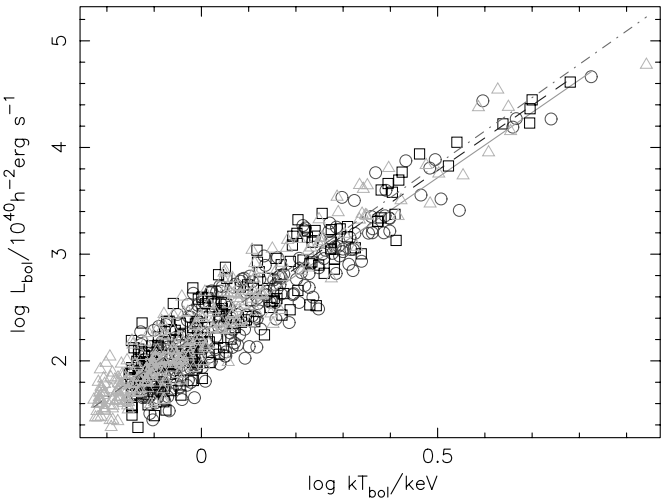

FIG. 4.—Bolometric luminosity-temperature relation within R_{500} at $z = 0$ of clusters in the three simulations. Symbols and lines are as in Fig. 2. [*See the electronic edition of the Journal for a color version of this figure.*]

the observations at low redshift ($z \sim 0$). Thus, based on the local scaling relations alone, we cannot easily discriminate between the source of the entropy excess in clusters: whether it is mainly due to radiative cooling, additional uniform heating at high redshift (prior to cluster formation), or localized heating from galaxy formation at all redshifts.

4.2. *Evolution of Scaling Relations with Redshift*

We now examine whether this degeneracy between models in the scaling relations at $z = 0$ can be broken by examining the cluster population at higher redshifts ($z = 0.5, 1, 1.5$). None of the relations require a significant variation in α with redshift. To make our results easier to interpret, therefore, we use simple power-law relations of the form given in equation (4) with α fixed at the $z = 0$ values given in Table 2.

To find the evolution of each relation, we first determine the normalizations, C_0, and their corresponding error bars, at each redshift in the same manner as described for redshift zero in § 4.1 above. We then minimize the χ^2 to obtain parameters Y_0 and A, as listed in Table 2, to fit the relation

$$\log C_0 = \log Y_0 + A \log (1 + z). \quad (12)$$

4.2.1. *Temperature-Mass Evolution*

In Figure 5, we present values of log (C_0) versus redshift for the three temperature-mass relations, with the best-fit straight line overplotted. For the T_{dyn}-M_{500} relation (*top panel*), we find similar evolution parameters for the three models, $A = 1.1$–1.2, confirming that including the effects of baryonic physics does not significantly affect cluster dynamics. The slight excess over the self-similar value of $A = 1$ is consistent with the changing cluster concentrations.

However, both the mass-weighted temperature (*middle panel*) and especially the emission-weighted temperature (*lower panel*) show significant variation between the three models. In each case the Feedback simulation approximately follows the scaling found for the dynamical temperature, with the Preheating and the Radiative simulations showing progressively larger deviations below the expected normalization as the redshift increases. The explanation for this lies in the variation of temperature of gas particles within each cluster and how this changes with redshift in the different models. We explore this further in § 5.

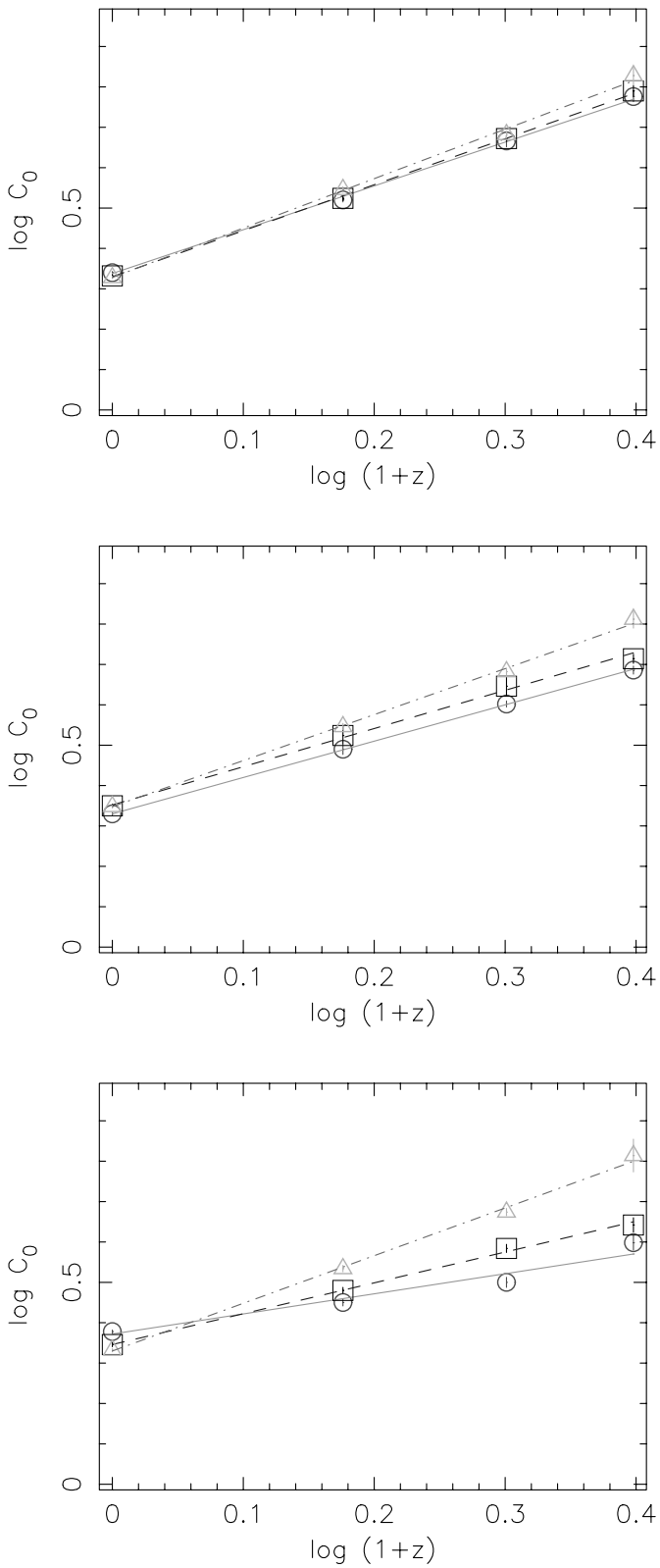

FIG. 5.—Normalization of the various temperature-mass relations as a function of redshift, for clusters in the Radiative (*solid line*), Preheating (*dashed line*), and Feedback (*dot-dashed line*) simulations, for the dynamical temperature (*top panel*), mass-weighted gas temperature (*middle panel*), and bolometric, emission-weighted temperature (*bottom panel*). [*See the electronic edition of the Journal for a color version of this figure.*]

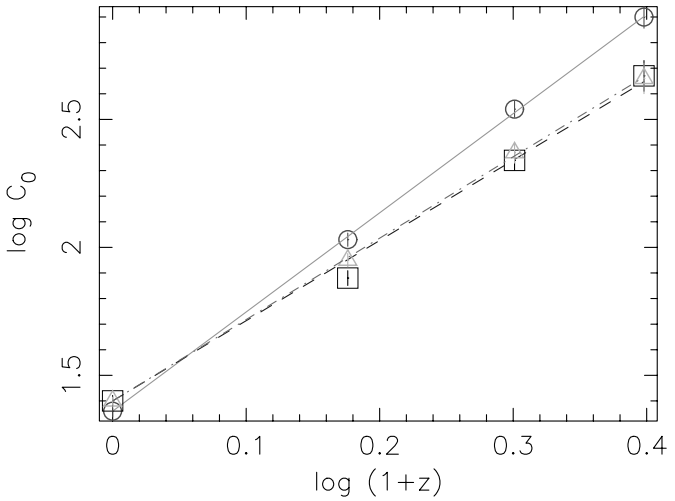

FIG. 6.—Normalization of the bolometric luminosity-mass relation as a function of redshift, for clusters in the Radiative (*solid line*), Preheating (*dashed line*), and Feedback (*dot-dashed line*) simulations. [*See the electronic edition of the Journal for a color version of this figure.*]

4.2.2. *Luminosity-Mass Evolution*

Figure 6 illustrates the normalization of the $L_{\rm bol}$-M_{500} relation versus redshift for all three models. The Preheating and Feedback models evolve almost identically with redshift ($A \sim 3$), but the Radiative run evolves more strongly ($A \sim 4$). These values bracket the self-similar value, $A = 3.5$; however, this agreement is somewhat coincidental because the slope of the relation at fixed redshift is much steeper than expected ($\alpha \sim 1.8$–2.1 rather than 1.3). The reason the Radiative simulation has steeper evolution is because of enhanced emission from cool gas at high redshift relative to that at low redshift; see discussion in § 5.

4.2.3. *Luminosity-Temperature Evolution*

Finally, we consider the evolution of the $L_{\rm bol}$-$T_{\rm bol}$ relation, with the relations at each redshift shown explicitly for each model in Figure 7 and the variation of normalization with redshift illustrated in Figure 8. It is interesting to note that the values of A are significantly different between all three models: the Feedback model predicts mildly negative evolution ($A = -0.6$), the Preheating mildly positive evolution ($A = 0.7$), and the Radiative strongly positive evolution ($A = 1.9$). The latter two models straddle the self-similar value ($A = 1.5$).

The difference in slopes between the Feedback and Preheating runs is driven by the differences in their temperature. The further difference between the Preheating and Radiative runs comes roughly equally from the temperature and luminosity evolution.

5. DISCUSSION

In this paper, we have focused on the evolution of cluster scaling relations in three simulations, each adopting a different model for nongravitational processes that affect the intracluster gas. In the first, the Radiative model, the gas could cool radiatively, and a significant fraction could cool down to low temperatures and form stars (MTKP02). In the Preheating model, the same is true even though the gas is additionally heated uniformly and impulsively by 1.5 keV per particle at $z = 4$ before cluster formation. In the third, the Feedback model, the heating rate was local and quasi-continuous, in proportion to the SFR from cooled gas. All three models are able to generate the required level of excess core entropy in order to reproduce the $L_{\rm X}$-$T_{\rm X}$ relation at $z = 0$ (MTKP02; KTJP04).

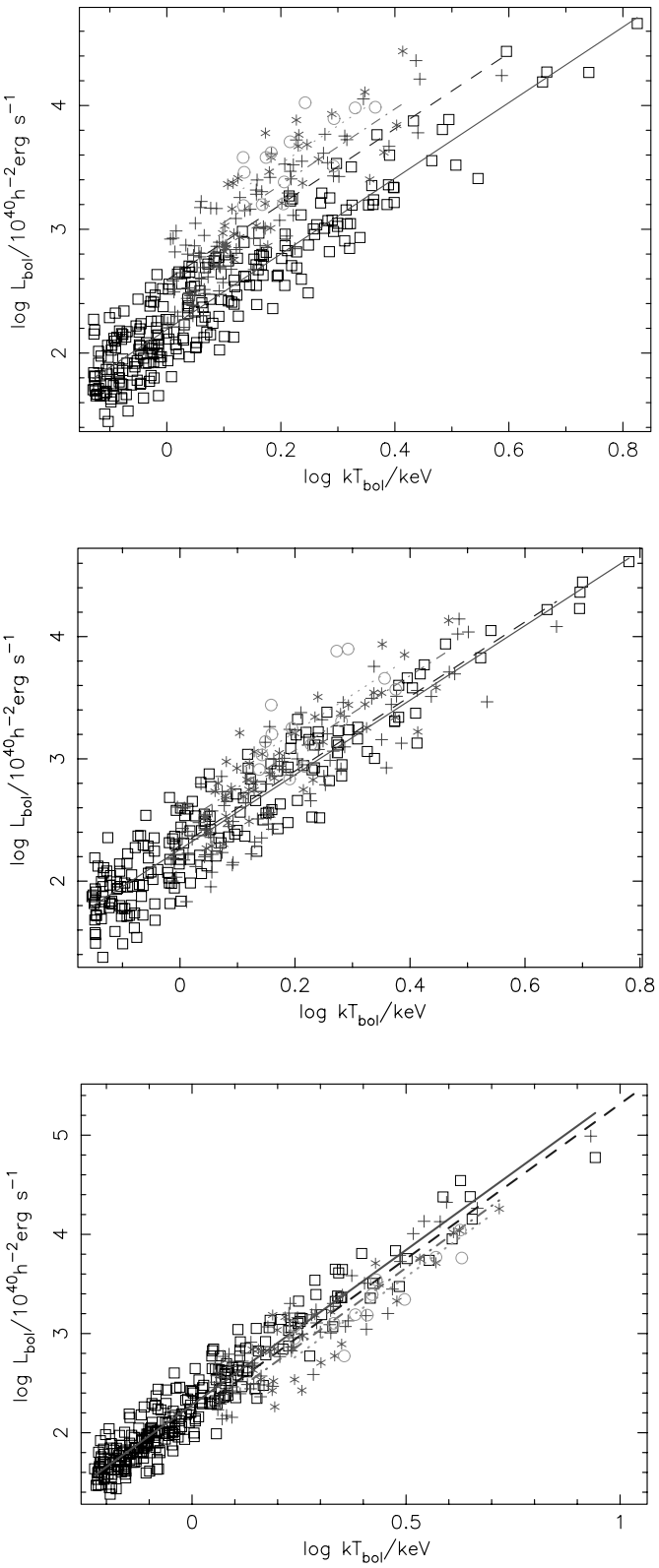

FIG. 7.—Bolometric luminosity-temperature relation for clusters at $z = 0, 0.5, 1, 1.5$ (*solid*, *dashed*, *dot-dashed*, *dotted lines, respectively*). The top panel is for the Radiative simulation, the middle for the Preheating simulation, and the bottom for the Feedback simulation. [*See the electronic edition of the Journal for a color version of this figure.*]

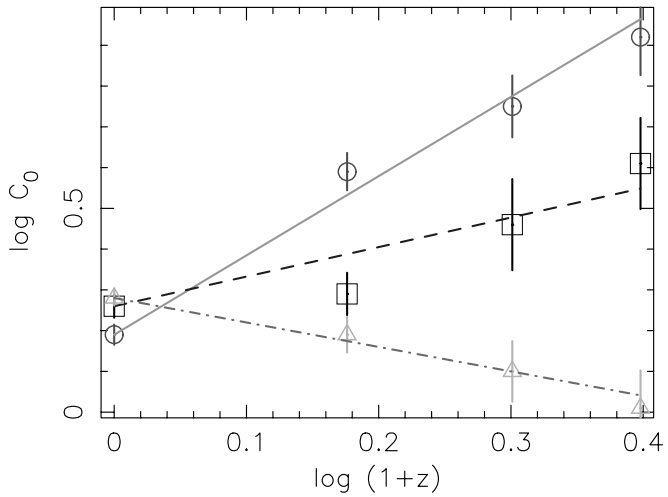

FIG. 8.—Normalization of the bolometric luminosity-temperature relation as a function of redshift, for clusters in the Radiative (*solid line*), Preheating (*dashed line*), and Feedback (*dot-dashed line*) simulations. [*See the electronic edition of the Journal for a color version of this figure*.]

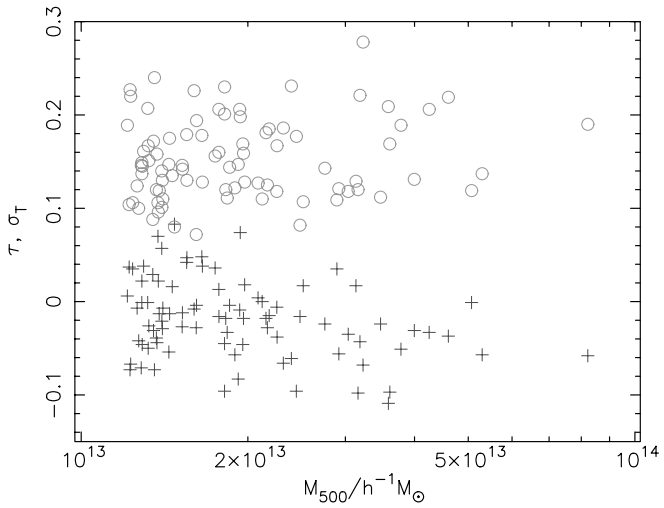

FIG. 9.—Values of τ (*crosses*) and σ_T (*circles*) for individual clusters in the Radiative simulation at $z = 1$. [*See the electronic edition of the Journal for a color version of this figure*.]

The most striking result presented in this paper is that the three models predict widely different L_X-T_X relations at high redshifts. The Radiative model predicts strongly positive evolution, the Preheating model mildly positive evolution, and the Feedback model, mildly negative evolution. At this point, it should be stressed that the values of A presented in Table 2 should not be taken too seriously. No attempt has been made to convert the bolometric, emission-weighted fluxes used in this paper to observable X-ray fluxes in different instrumental bands. Also, the volume of our simulation boxes is such that we only get a modest number of relatively poor clusters at high redshift. Nevertheless, the qualitative difference between the models is very encouraging and suggests that evolution of X-ray properties may act as a strong discriminant between models in the future.

Previous work (e.g., Pearce et al. 2000; Muanwong et al. 2001) has made great play of the fact that radiative cooling can remove low-entropy material and lead to a raising of the gas temperature above the virial temperature of the host halo. That effect is reproduced by the Radiative simulation in this paper, but it is interesting to note that the bolometric X-ray temperature exceeds the dynamical temperature of the clusters only at very low redshift, $z \lesssim 0.1$. At higher redshifts it falls below the dynamical temperature and is a factor of 1.6 lower by $z = 1.5$. This departure from self-similarity is a consequence of the changing density parameter, Ω, in the concordance ΛCDM cosmology: at high redshift Ω is close to unity and structures grow freely; at lower redshifts Ω falls well below unity and the rate of growth of cosmic structures declines.

The behavior of the Preheating simulation is similar, although the relative decline in the ratio of the gas to the dynamical temperature is smaller. The effect cannot, therefore, be due to the cooling of intracluster gas in the cluster cores between a redshift of 1.5 and the present; in the Preheating run very little gas cools below a redshift of 4, and so that cool core gas would still be there today. Instead, we attribute the presence of cool gas to the accretion of low-temperature subclumps. Such accretion is a ubiquitous feature of clusters (e.g., Rowley et al. 2004). Cool gas is seen in maps of clusters at low redshift (Onuora et al. 2003) and would be expected to be much more prevalent in clusters at high redshift in the ΛCDM cosmology.

To test this hypothesis, we measured the temperature variation within each cluster as follows. First, we averaged properties within 20 spherical annuli out to R_{500} to create smoothed dynamical, $\bar{T}_{\rm dyn}$, and gas temperature, $\bar{T}_{\rm gas}$, profiles. Then we measured the mean deviation (in log space) of the gas temperature from the local dynamical temperature,

$$\tau = \frac{1}{N}\sum_i \left(\log T_i - \log \bar{T}_{\rm dyn}\right), \tag{13}$$

and the rms deviation of the temperature, σ_T, from the mean,

$$\sigma_T^2 = \frac{1}{N}\sum_i \left(\log T_i - \log \bar{T}_{\rm gas}\right)^2, \tag{14}$$

where $N = \sum_i$ and the sum runs over all hot gas particles ($T_i > 10^5$ K) within R_{500}.

As an example, Figure 9 shows the values of τ (*crosses*) and σ_T (*circles*) for each cluster at $z = 1$ in the Radiative simulation. This particular example has been chosen simply because the two properties are well separated and easy to distinguish on the plot. As can be seen, the mean gas temperature of the more massive clusters typically lies below the local dynamical temperature by as much as 15% at this redshift. However, the dispersion in temperature is much larger, typically a factor of 1.5, so there will be fluctuations both above and below the dynamical temperature.

Figure 10 demonstrates visually the evolution of τ and σ_T with redshift. At each redshift, the plot shows the average value of τ over all clusters with masses greater than $1.2 \times 10^{13}\, h^{-1}\, M_\odot$. The half-width of the shaded regions represent the average values of σ_T, divided by 10 for clarity. Concentrating first on the Radiative simulation, it can be seen that the mean cluster temperature increases relative to the virial temperature over time and that the dispersion in temperature decreases. This is consistent with a decreasing amount of substructure within the clusters at lower redshift, although it should be noted that part of the effect is due to the narrower range of cluster masses resolved by the simulations at high redshift, as the average value of τ decreases with increasing cluster mass.

The behavior of the Preheating simulation mimics that of the Radiative one, but with a bias to higher mean temperatures. The Feedback simulation, however, is quite different. It shows a much larger dispersion than the other two, but no bias to low temperatures at high redshift. That is because gas is free to cool down to

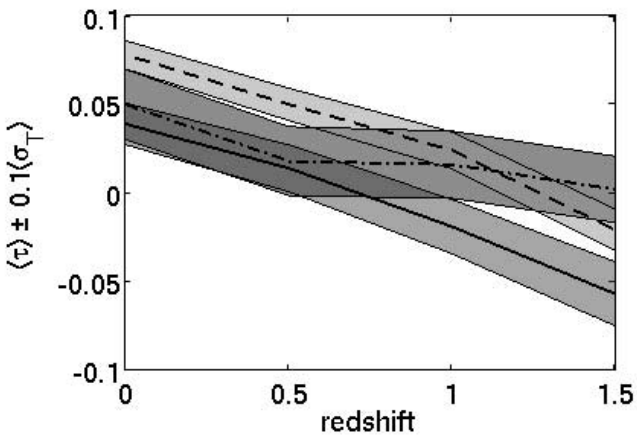

FIG. 10.—Mean value of τ for clusters in the Radiative (*solid line*), Preheating (*dashed line*), and Feedback (*dash-dotted line*) simulations as a function of redshift. The half-width of the shaded regions corresponds to the mean value of σ_T at that redshift. All averages are for clusters with mass greater than $1.2 \times 10^{13}\ h^{-1}\ M_\odot$. [*See the electronic edition of the Journal for a color version of this figure.*]

low temperatures, but some of that gas is then heated back up high temperatures by the feedback. At low redshift cooling becomes less important and the Feedback run then shows a slight rise in τ, matching that seen in the other two runs.

Our results have two very important implications for observations of high-redshift clusters. Firstly, the behavior of the L_X-T_X relation at high redshift will determine the number of high-redshift clusters to be found in surveys such as the ongoing *XMM-Newton* Cluster Survey (Romer et al. 2001) and this will have a significant impact on their use in probing cosmological parameters. A positive evolution such as that shown by the Radiative simulation will yield many more observable high-redshift clusters than the negative evolution of the Feedback model. As discussed in § 2 and summarized in Figure 1, the observational situation is far from clear but does seem to indicate positive evolution.

Turning this argument around, our results suggest that observational constraints on the degree of evolution of the L_X-T_X relation will allow interesting constraints to be placed on the source of entropy generation in clusters, in particular the relative role of cooling and heating and whether most of the heating of the intracluster gas occurred at high redshift (as in the Preheating model) or was a continuous function of redshift (as in the Feedback model). Taking our results at face value with recent observations would suggest that our Feedback model is generating too much excess entropy at $z < 1.5$ and that the bulk of the heating must have occurred at higher redshift. However, we stress once again that this result is very tentative.

6. CONCLUSIONS

The evolution of X-ray cluster scaling relations are a crucial component when constraining cosmological parameters with clusters. Observational studies at low redshift have already shown that the scaling relations deviate from self-similar expectations (attributed to nongravitational heating and cooling processes), but their redshift dependence is only starting to be explored. In this paper we have investigated the sensitivity of the X-ray scaling relations to the nature of heating processes, using three numerical simulations of the ΛCDM cosmology with different heating models. While all three simulations reproduce more or less the same scaling relations at $z = 0$ (as they were designed to produce the correct level of excess entropy), they predict significantly different results for the evolution of the L_X-T_X relation to $z = 1.5$.

In conclusion, our findings strongly suggest that the relative abundance of high- and low-redshift clusters will place interesting constraints on the nature of nongravitational entropy generation in clusters. First indications are that an early and widespread preheating of the ICM is to be preferred to an extended period of preheating, as is associated with galaxy formation. However, much more detailed modeling is required, and the observational picture is as yet unclear.

The simulations described in this paper were carried out on the Cray-T3E at the Edinburgh Parallel Computing Centre and the COSmology MAchine in Durham as part of the Virgo Consortium investigations into the formation of structure in the Universe. O. M. is grateful for the hospitality and support of the Astronomy Centre at the University of Sussex where much of the work in this paper was carried out, and for financial support from Khon Kaen University. She and P. A. T. also acknowledge support from the Thailand Research Fund and the Commission on Higher Education grant MRG4680129.

REFERENCES

Allen, S. W., & Fabian, A. C. 1998, MNRAS, 297, L57
Allen, S. W., Schmidt, R. W., Fabian, A. C., & Ebeling, H. 2003, MNRAS, 342, 287
Arnaud, M., Aghanim, N., & Neumann, D. M. 2002, A&A, 389, 1
Balogh, M. L., Babul, A., & Patton, D. R. 1999, MNRAS, 307, 463
Borgani, S., Governato, F., Wadsley, J., Menci, N., Tozzi, P., Quinn, T., Stadel, J., & Lake, G. 2002, MNRAS, 336, 409
Borgani, S., et al. 2001, ApJ, 561, 13
———. 2004, MNRAS, 348, 1078
Bower, R. G. 1997, MNRAS, 288, 355
Bower, R. G., Benson, A. J., Lacey, C. G., Baugh, C. M., Cole, S., & Frenk, C. S. 2001, MNRAS, 325, 497
Bryan, G. L. 2000, ApJ, 544, L1
Davé R., Katz, N., & Weinberg, D. H. 2002, ApJ, 579, 23
Edge, A. C., & Stewart, G. C. 1991, MNRAS, 252, 414
Eke, V. R., Cole, S., & Frenk, C. S. 1996, MNRAS, 282, 263
Ettori, S., Tozzi, P., Borgani, S., & Rosati, P. 2004, A&A, 417, 13
Evrard, A. E., & Henry, J. P. 1991, ApJ, 383, 95
Fairley, B. W., Jones, L. R., Scharf, C., Ebeling, H., Perlman, E., Horner, D., Wegner, G., & Malkan, M. 2000, MNRAS, 315, 669
Henry, J. P. 1997, ApJ, 489, L1
———. 2000, ApJ, 534, 565
———. 2004, ApJ, 609, 603
Henry, J. P., & Arnaud, K. A. 1991, ApJ, 372, 410
Holden, B. P., Stanford, S. A., Squires, G. K., Rosati, P., Tozzi, P., Eisenhardt, P., & Spinrad, H. 2002, AJ, 124, 33
Horner, D. J., Mushotzky, R. F., & Scharf, C. A. 1999, ApJ, 520, 78
Kaiser, N. 1986, MNRAS, 222, 323
———. 1991, ApJ, 383, 104
Kay, S. T., Thomas, P. A., Jenkins, A., & Pearce, F. R. 2004, MNRAS, 355, 1091 (KTJP04)
Kay, S. T., Thomas, P. A., & Theuns, T. 2003, MNRAS, 343, 608
Knight, P. A., & Ponman, T. J. 1997, MNRAS, 289, 955
Kotov, O., & Vikhlinin, A. 2005, ApJ, 633, 781
Kravtsov, A. V., & Yepes, G. 2000, MNRAS, 318, 227
Loewenstein, M. 2000, ApJ, 532, 17
Lumb, D. H., et al. 2004, A&A, 420, 853
Markevitch, M. 1998, ApJ, 504, 27
Maughan, B. J., Jones, L. R., Ebeling, H., & Scharf, C. 2006, MNRAS, 365, 5090
Mazzotta, P., Rasia, E., Moscardini, L., & Tormen, G. 2004, MNRAS, 354, 10
McCarthy, I. G., Balogh, M. L., Babul, A., Poole, G. B., & Horner, D. J. 2004, ApJ, 613, 811
Metzler, C. A., & Evrard, A. E. 1994, ApJ, 437, 564
Muanwong, O., Thomas, P. A., Kay, S. T., & Pearce, F. R. 2002, MNRAS, 336, 527 (MTKP02)

Muanwong, O., Thomas, P. A., Kay, S. T., Pearce, F. R., & Couchman, H. M. P. 2001, ApJ, 552, L27
Mushotzky, R. F., & Scharf, C. A. 1997, ApJ, 482, L13
Novicki, M. C., Sornig, M., & Henry, J. P. 2002, AJ, 124, 2413
Onuora, L., Kay, S. T., & Thomas, P. A. 2003, MNRAS, 341, 1246
Pearce, F. R., Thomas, P. A., Couchman, H. M. P., & Edge, A. C. 2000, MNRAS, 317, 1029
Pierpaoli, E., Borgani, S., Scott, D., & White, M. 2003, MNRAS, 342, 163
Pierpaoli, E., Scott, D., & White, M. 2001, MNRAS, 325, 77
Ponman, T. J, Cannon, D. B., & Navarro, J. F. 1999, Nature, 397, 135
Rasia, E., Mazzotta, P., Borgani, S., Moscardini, L., Dolag, K., Tormen, G., Diaferio, A., & Murante, G. 2005, ApJ, 618, L1
Romer, A. K., Viana, P. T. P., Liddle, A. R., & Mann, R. G. 2001, ApJ, 547, 594
Rowley, D. R., Thomas, P. A., & Kay, S. T. 2004, MNRAS, 352, 508
Seljak, U. 2002, MNRAS, 337, 769
Sutherland, R. S., & Dopita, M. A. 1993, ApJS, 88, 253
Tornatore, L., Borgani, S., Springel, V., Matteucci, F., Menci, N., & Murante, G. 2003, MNRAS, 342, 1025
Tozzi, P., & Norman, C. 2001, ApJ, 546, 63
Valdarnini, R. 2003, MNRAS, 339, 1117
Viana, P. T. P., Kay, S. T., Liddle, A. R., Muanwong, O., & Thomas, P. A. 2003, MNRAS, 346, 319
Viana, P. T. P., & Liddle, A. R. 1996, MNRAS, 281, 323
———. 1999, MNRAS, 303, 535
Vikhlinin, A. 2006, ApJ, 640, 710
Vikhlinin, A., VanSpeybroeck, L., Markevitch, M., Forman, W. R., & Grego, L. 2002, ApJ, 578, L107
Voit, G. M., Balogh, M. L., Bower, R. G., Lacey, C. G., & Bryan, G. L. 2003, ApJ, 593, 272
Voit, G. M., & Bryan, G. L. 2001, Nature, 414, 425
Voit, G. M., Bryan, G. L., Balogh, M. L., & Bower, R. G. 2002, ApJ, 576, 601
White, D. A., Jones, C., & Forman, W. 1997, MNRAS, 292, 419
White, S. D. M., Efstathiou, G., & Frenk, C. S. 1993, MNRAS, 262, 1023
Wu K. K. S., Fabian, A. C., & Nulsen, P. E. J. 2000, MNRAS, 318, 889
Wu X.-P., & Xue, Y.-J. 2002, ApJ, 569, 112
Xue, Y.-J., & Wu X.-P. 2000, ApJ, 538, 65